Wiley InterScience — Discover Something Great
Early View publication on www.interscience.wiley.com (issue and page numbers not yet assigned; citable using Digital Object Identifier – **DOI**)
phys. stat. sol. (c), 1–6 (2008) / **DOI** 10.1002/pssc.200778558
physica status solidi c — www.pss-c.com — *current topics in solid state physics*

# Growth mechanism of catalyst- and template-free InN nanorods

**Yong Sun Won, Young Seok Kim, Olga Kryliouk*, and Tim Anderson**

Department of Chemical Engineering, University of Florida, Gainesville, FL32611, USA

Received 27 September 2007, revised 4 December 2007, accepted 26 December 2007
Published online 10 April 2008

**PACS** 31.15.E–, 34.50.Lf, 62.23.Hj, 81.05.Ea, 81.15.Gh, 82.60.–s

* Corresponding author: e-mail Olga_Kryliouk@amat.com, Phone: 1-408-235-6033, Fax: 1-408-235-6263

A feasible mechanism for catalyst- and template-free InN nanorod growth was proposed, consisting of the random nanoparticle nucleation from stable gas phase oligomers and the subsequent directional growth along the c-axis. A combined study of equilibrium analysis and computational thermochemistry was used to determine the optimal growth conditions – growth temperature and Cl/In ratio – for InN nanorod growth based on the proposed mechanism, and the computationally determined values showed a good agreement with reported experimental results. The involvement of $InCl_3$ as a key species in the proposed mechanism required the Cl/In ratio to be ~ 3 by stoichiometry. The growth zone of InN nanorods by HVPE was demonstrated to lie in the vicinity of the growth-etch transition.

© 2008 WILEY-VCH Verlag GmbH & Co. KGaA, Weinheim

**1 Introduction** Nanoscale structures (such as nanowires and nanorods) of group III-nitride materials have drawn extensive interest in the application of quantum electronics, optoelectronics and sensors [1-8]. We already demonstrated the promising application of Pt-coated InN nanorods (termed NRs hereafter) for hydrogen gas sensors [9]. In many cases, group III-nitride nanorods have been grown by catalyst-assisted or oxide-assisted vapor phase growth techniques [10-14]. Only limited attempts of catalyst-, oxide-, and template-independent group III-nitride NR growth were successfully reported; GaN NR growth by typical hydride vapor phase epitaxy (HVPE) [15], InN NR growth by hydride metal organic vapor phase epitaxy (H-MOVPE) from our efforts [9, 16], and AlN NR growth by chemical vapor deposition (CVD) using $AlCl_3$ and $NH_3$ [17]. A proper growth mechanism hence has not yet been proposed unlike catalyst-assisted and oxide-assisted growths described by the vapor-liquid-solid mechanism and vapor-solid mechanism involving a series of oxidation and reduction respectively [14].

Meanwhile, Timoshkin pointed out the possibility of gas phase nanoparticle formation in his theoretical study on the stability of rings and clusters in the gas phase during the CVD of group III-V materials [18]. Several other theoretical studies of potential gas phase intermediates in group III element (Al, Ga, and In)-N-H-Cl systems also suggested the formation of thermodynamically stable oligomer species, $[Cl_2(Al, Ga\ or\ In)NH_2]_n$, in the gas phase even at elevated temperatures (up to 1000 K) [19-22]. Based on those conclusions [18-22], a probable solid-vapor mechanism for InN NR growth by H-MOVPE featured with random nanoparticle nucleation from the stable gas phase oligomers and the subsequent directional growth along the c-axis was introduced in our previous report [16]. Experimental observations were fairly consistent with the proposed growth mechanism as well [16].

In this study, the proposed solid-vapor mechanism [16] is rationalized in more details using equilibrium analysis combined with computational thermochemistry. The optimal growth conditions for InN NR growth are resolved by evaluating kinetic and thermodynamic constraints of the system. Computationally determined growth conditions are then compared to reported experimental conditions in literature [16] to verify the mechanism, particularly growth temperature and Cl/In ratio which were experimentally screened out as most influencing growth parameters [16].

**2 Computational methods** All computational thermochemistry calculations were carried out using the GAUSSIAN 03 program [23], along with B3LYP DFT model chemistry and a split basis set (LanL2DZ for In element and 6-311G(d) for other elements) [23-25]. Full

geometry optimization was carried out for all gas species. The transition state (TS) was located using the Berny Algorithm as implemented in the GAUSSIAN 03 program [23]. Harmonic vibration frequencies were calculated for each structure, which allowed the enthalpy and Gibbs energy to be obtained computationally.

The CVD diagrams were computed using *ThermoCalc* software with the SUB94 database implemented [26-29].

## 3 Results and discussion

**3.1 Growth mechanism of InN nanorods** The growth mechanism of catalyst- and template-free InN NRs by H-MOVPE is proposed as shown in Fig. 1. In this modified system of HVPE, HCl is reacted with trimethylindium (TMIn) instead of the liquid indium source used in conventional HVPE [16]. The original idea of the proposed mechanism is the possibility of the nucleation of nanoparticles from stable gas phase oligomer species, $[Cl_2InNH_2]_n$. The oligomer is an aggregate of the monomer ($Cl_2InNH_2$) with HCl eliminated from the ammonia adduct ($Cl_3In:NH_3$).

As shown in Fig. 1, 2-D film growth with uniform nucleation by the reaction of InCl (ad) and $NH_3$ (ad) is favored when the Cl/In ratio is ~ 1. In this region, InCl is the dominant gas phase reactant species along with $NH_3$. When the Cl/In ratio is increased to 3, the formation of $InCl_3$ becomes kinetically possible depending on the growth temperature (> 800 K) although its negative entropy generation ($\Delta S < 0$) renders it thermodynamically unfavorable with the temperature increase. It is discussed in Sections 3.2 and 3.3. The $InCl_3$ forms an ammonia adduct ($Cl_3In:NH_3$) with $NH_3$ and the subsequent monomer formation ($Cl_2InNH_2$) via a HCl elimination leads to the formation of innate In-N bond in monomer [18-22]. The oligomer species ($[Cl_2InNH_2]_n$), an aggregate of monomers, has been identified to be stable in the gas phase below a certain high temperature (up to 1000 K) [18-22]. The strong intramolecular H–Cl hydrogen bonding and dipole-dipole interactions are known to favor the formation of larger oligomer species [21]. The extent of the oligomerization process has not been known explicitly, but Timoshkin reported that the generation of gas phase $[HGaNH]_n$ clusters even with oligomerization degree $n \geq 60$ is viable in his theoretical works [30, 31]. When the Cl/In ratio becomes much higher than 3, InN growth becomes unfavorable because of the enhanced HCl etching by excess HCl (g). In addition, the equilibrium of the reaction, $InCl_3:NH_3 \leftrightarrow Cl_2InNH_2 + HCl$, is shifted against the monomer formation. The result is either sparse nucleation or a complete lack of InN growth.

The proposed growth mechanism presented in Figure 1 properly describes the growth behavior observed in the InN NR growth by H-MOVPE [16]. The involvement of $InCl_3$ as a key intermediate in the mechanism requires the Cl/In ratio to be ~ 3 by stoichiometry and this has been confirmed experimentally, as the optimal Cl/In ratio used for InN NR growth was 3 ~ 4 [16]. At higher chlorine concentration in the system (Cl/In = 4 ~ 7), sparse nanorods or microrods were grown [16]. In addition, the growth behavior of InN NRs was independent of the kind of substrate (silicon, GaN, or sapphire) [16]. This explains in that the nucleation of nanoparticles from stable gas phase oligomers, regardless of the growth mechanism, would not be likely related to the substrate.

The observations that an individual nanorod was faceted and did not show any cap morphology, and its diameter did not change along the growth direction suggested a solid-vapor mechanism initiated by random nanoparticle nucleation and the subsequent directional growth [16]. The preferential growth along the c-axis [15-17] is rather explicitly portrayed by dipole-dipole interactions between

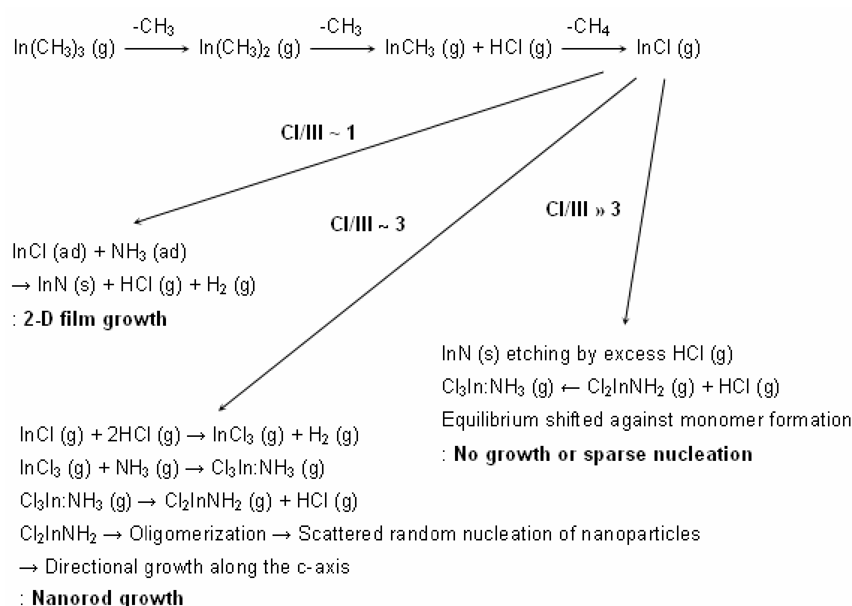


**Figure 1** Proposed growth mechanism of InN NRs by H-MOVPE.

© 2008 WILEY-VCH Verlag GmbH & Co. KGaA, Weinheim

nanoparticle nuclei and gas phase precursor species along the c-axis. An oligomer species ($Cl_9In_6N_6H_9$) [21], as an example, has the wurtzite structure inside although its boundaries are saturated with hydrogens and chlorines. The nanoparticle nucleus resulting from this oligomer species thus has a dipole axis along the c-axis of its incorporated wurtzite structure. It is likely that the dipole axes of nuclei then are randomly oriented at the initial stage of nucleation irrespective of the kind of substrate. Chlorine containing gas phase precursor species have strong dipoles, as does $NH_3$. Thus, higher reactant flux driven by dipole-dipole interactions along the c-axis favors the directional growth following randomly oriented nanoparticle nucleation. The experimental results demonstrated that the growth rate along the c-axis is significantly higher than the rate along the lateral direction [15-17]. It has also been demonstrated that preferential growth of ZnO nanorods along the c-axis in the presence of a perpendicular electric field in plasma-enhanced CVD occurs by attracting charged particles to the nanorod ends [32], and this is in the same context.

**3.2 Gas phase kinetics** The growth temperature was experimentally confirmed as a key growth parameter along with Cl/In ratio [16]. While the preferable Cl/In ratio for the NR growth was determined to be ~ 3 by the inherent idea of the proposed growth mechanism itself (see Fig. 1), a combined study of computational thermochemistry and equilibrium analysis was employed to locate the temperature range most preferable for InN NR growth based on the proposed mechanism, and the results are discussed in Sections 3.2 and 3.3. In most cases, kinetically limited gas phase reactions placed an upper limit on growth temperature in CVD. The detailed study using computational thermochemistry thus was preceded to obtain activation barriers of gas phase reactions and to assess kinetic constraints of the system in terms of growth temperature.

To test the selected basis set of moderate size (LanL2DZ for In element and 6-311G(d) for other elements), reaction enthalpies for the thermal decomposition process, TMIn → dimethylindium (DMIn) → monomethylindium (MMIn), as occurred initially in H-MOVPE [16], were calculated and compared with literature values [33] obtained with a bigger basis set in Table 1. It was demonstrated the selected basis set is acceptable enough to describe the trend of enthalpies for the methyl dissociation from TMIn with a fair accuracy. The DMIn has the planar doublet $C_{2v}$ geometry with an unpaired electron due to their $sp^2$ hybridization and it is likely to decompose readily to stable singlet MMIn, where one electron in the *p* orbital is in effect donated to the carbon. The Mulliken atomic charges of In and C elements (In/C) were varied in DMIn and MMIn as follows: 0.601/-0.196 (DMIn) → 0.445/-1.069 (MMIn). The MMIn is stabilized by the ionic characteristics of In-C bond. The energy barrier for the third methyl dissociation from MMIn is increased again due to their strong In-C bond.

**Table 1** Calculated reaction enthalpies for the thermal decomposition of TMIn.

| Entry | Reactions | $\Delta H^o_{298}$ (kcal/mol) | $\Delta H^o_{298}$ in literature |
|---|---|---|---|
| 1 | $In(CH_3)_3 \rightarrow In(CH_3)_2 + \cdot CH_3$ | 61.1 | 58.8[a] |
| 2 | $In(CH_3)_2 \rightarrow InCH_3 + \cdot CH_3$ | 26.6 | 24.7[a] |
| 3 | $InCH_3 \rightarrow In + \cdot CH_3$ | 54.0 | 53.8[a] |

[a]Data was taken from Ref. [33].

The formation of InCl via the reaction of MMIn and HCl, known to occur in H-MOVPE, is depicted in Fig. 2. The calculated energetics showed a minimum barrier for the reaction and its high exothermicity shifted the reaction forward. The main gas species, with Cl/In ratio ~ 1, becomes InCl. The 2-D film growth then follows via a heterogeneous reaction between adatoms of InCl and $NH_3$. In HVPE, liquid In reacts with HCl to form InCl.

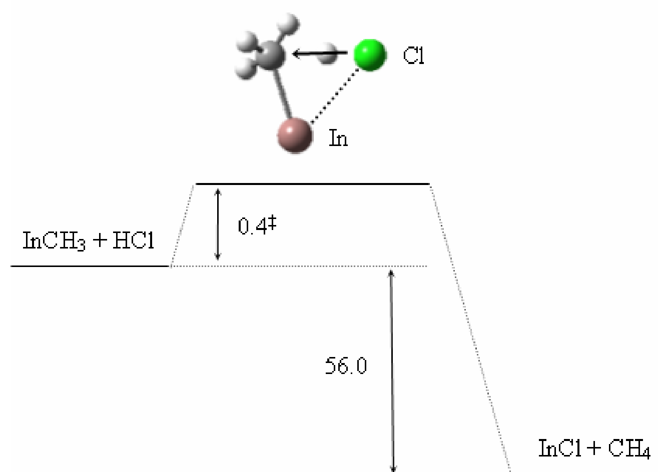


**Figure 2** Calculated energetics of the formation of InCl. The $\Delta U^{\circ}_{298}$ values have the unit of kcal/mol.

When the Cl/In ratio increases up to 3, another pathway becomes viable in the gas phase, the formation of $InCl_3$. Figure 3 showed the calculated energetics of $InCl_3$ formation from InCl via the reaction with two HCls. The overall reaction is also exothermic with negative ΔS. This means the pathway is thermodynamically favorable below a certain temperature, which is discussed in Section 3.3. The pathway did have a comparatively high activation barrier in the first HCl addition to form $InHCl_2$, probably attributed to the bond characteristic change from ionic to $sp^2$ hybridized. $InHCl_2$ and $InCl_3$ have planar $C_{2v}$ and $C_{3h}$ symmetries by $sp^2$ hybridization, respectively.

The formation of ammonia adduct ($Cl_3In:NH_3$) readily follows due to its high exothermicity. Table 2 listed calculated reaction enthalpies for the formation of $Cl_3In:NH_3$ and corresponding literature value obtained using a higher level MP2 theory [20]. They also showed a good agreement. Although the subsequent monomer formation


© 2008 WILEY-VCH Verlag GmbH & Co. KGaA, Weinheim

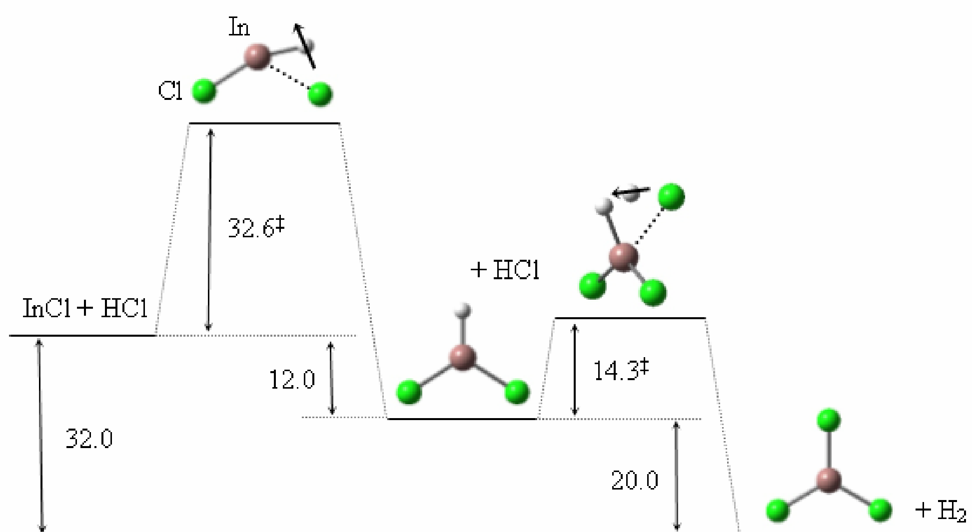


**Figure 3** Calculated energetics of the formation of $InCl_3$. The $\Delta U^{\circ}_{298}$ values have the unit of kcal/mol.

through HCl elimination is endothermic, its reaction enthalpy is smaller than the energy gained in the corresponding ammonia adduct formation [20]. This suggests that a HCl elimination can easily occur in the gas phase as long as the condition is met that the ammonia adduct formation is thermodynamically and kinetically favorable. Okamoto [20] meanwhile reported that the activation energy for monomer formation is 'not much larger than the reaction energy' and Timoshkin [21] found that the TS (Transition State) for a HCl elimination from $GaCl_3$:$NH_3$ lies only 1 kJ/mol (SCF/pVDZ level) higher than the reaction energy.

**Table 2** Reaction enthalpies for the formation of ammonia adduct ($Cl_3In$:$NH_3$): Calculated and literature values.

| Reactions | $\Delta H^{\circ}_{298}$ (kcal/mol) | $\Delta H^{\circ}_{298}$ in literature |
|---|---|---|
| $InCl_3 + NH_3 \rightarrow Cl_3In{:}NH_3$ | -36.9 | -35.9[a] |

[a]Data was taken from Ref. [20].

In summary, there are two kinetically limited steps in gas phase reactions in the mechanism proposed in Fig. 1; the first methyl dissociation from TMIn and the first HCl insertion into InCl to form $InHCl_2$. The former was attributed to the huge bond dissociation energy as shown in Table 1, while the latter was a bimolecular reaction (two moles of reactants → one mole of transition state, $\Delta S^{\circ,\ddagger} < 0$) having a fairly high activation energy as depicted in Fig. 3. Table 3 summarizes $\Delta G^{\circ,\ddagger}$ and rate constants of those reactions at several temperatures. The absolute rate equations from transition state theory (TST) were used for the calculation of rate constants as shown below [34]. For where no obvious transition states exist (entry 1/3), it was assumed $\Delta H^{\circ} = \Delta H^{\circ,\ddagger}$ and $\Delta S^{\circ} = \Delta S^{\circ,\ddagger}$.

$$k_{unimolecular} = (k_B T/h) \exp(-\Delta G^{\circ,\ddagger}/RT)$$

$$k_{bimolecular} = (k_B T/h) (RT/P^{\circ}) \exp(-\Delta G^{\circ,\ddagger}/RT)$$

where $k_B$, h, R are Boltzmann constant, Plank constant, and gas constant respectively and $P^{\circ}$ = 1 atm.

**Table 3** Calculated activation energies and rate constants for selected reactions at several different temperatures.

| Entry | Reactions | $\Delta S^{\circ,\ddagger}_{298}$ (cal/mol-K) | $\Delta H^{\circ,\ddagger}_{298}$ (kcal/mol) | $\Delta G^{\circ,\ddagger}/k$[a] (298 K) | $\Delta G^{\circ,\ddagger}/k$[a] (800 K) | $\Delta G^{\circ,\ddagger}/k$[a] (1300 K) |
|---|---|---|---|---|---|---|
| 1 | $In(CH_3)_3 \rightarrow In(CH_3)_2 + \cdot CH_3$ | 37.8 | 61.1 | 49.8/ $1.8\times10^{-25}$ | 31.0/ $5.6\times10^{+5}$ | 13.0/ $1.8\times10^{+12}$ |
| 2 | $InCl + HCl \rightarrow [InCl{\cdot}HCl]^{\ddagger}$ | -26.5 | 32.0 | 39.9/ $2.1\times10^{-15}$ | 53.2/ 3.2 | 66.2/ $2.1\times10^{+5}$ |
| 3 | $InCl_3 + NH_3 \rightarrow InCl_3{:}NH_3$ | -33.3 | -36.9 | -26.9/ $3.5\times10^{+33}$ | -10.7/ $1.4\times10^{+17}$ | 4.3/ $5.2\times10^{+13}$ |

[a]$\Delta G^{o,\ddagger}$ values have the unit of kcal/mol. The rate constants have the unit of 1/sec for unimolecular reaction and liter/mol-sec for bimolecular reaction, respectively.

© 2008 WILEY-VCH Verlag GmbH & Co. KGaA, Weinheim 

Although rate constants listed in Table 3 are not suitable for rigorous analysis, they demonstrated a certain high temperature (> 800 K) is required for the two kinetically limited reactions (entry 1/2), especially the HCl addition to InCl, to have rate constants of some orders of magnitude and be kinetically accessible. The ammonia adduct formation (entry 3) was shown to be facile even at high temperature despite its high negative entropy generation ($\Delta S^{\circ,\ddagger}_{298}$ < 0) due to its high exothermicity ($\Delta H^{\circ,\ddagger}_{298}$ < 0).

**3.3 Temperature dependency of InN NR growth** A kinetic constraint was addressed in Section 3.2 that a certain high temperature (> 800 K) is needed to activate the formation of $InCl_3$ as a key species in the growth mechanism proposed in Figure 1. It however comes in conflict with the high degree of InN etching in a chlorinated environment at high temperature.

A CVD phase diagram for InN growth with Cl/In ratio versus growth temperature was presented in Fig. 4. The recently assessed data by Leitner *et al*. [35] with well supported experimental results provided that a thermal decomposition temperature of solid InN (~ 680 K) is lower than the typical growth temperature (~ 800 K) of InN films [35, 36]. The InN NR growth by H-MOVPE [16] was thus apparently achieved under non-equilibrium conditions because the thermodynamic constraint does not allow for the formation of InN. A CVD phase diagram presented in Fig. 4 was in fact fitted to match with the experimental result of InN NR growth by H-MOVPE [16], The phase transition temperature is around 800 K when a Cl/Ga ratio is ~ 3, which is still a bit lower than the optimum growth temperature range (around 900 K) experimentally observed for InN NR growth [16]. The Gibbs energy for solid InN was taken from *ThermoCalc* SUB94 database. This is corresponding to lowering the Gibbs energy by ~ 16 kcal/mol compared to the data assessed by Leitner *et al*. The lowering of the Gibbs energy of InN in Figure 4 could be understood to consider kinetic barrier for decomposition because decomposition temperature and growth temperature generally have a large overlap due to kinetic barriers. However, it is noted that the optimized growth temperature for InN NR growth was confined to a very narrow range, 600 to 650 °C (873 to 923 K) [16]. Considering that the InN film growth using the same H-MOVPE system - where InCl is dominant in the gas phase - was possible at temperatures as low as 500 to 550 °C (773 to 823 K) [36], the temperature range from 600 to 650 °C was likely determined by the kinetic constraint for $InCl_3$ formation (see Table 3). The high degree of InN etching (thermodynamic constraint) suppressed the growth temperature within the narrow range where the kinetic constraint is barely removed. An increase of the N/In ratio lifted the phase transition temperature at a given Cl/In ratio. The growth zone of InN NRs by H-MOVPE however lied in the vicinity of the growth-etch transition in general as shown in Fig. 4 and reported in our experimental work [16].

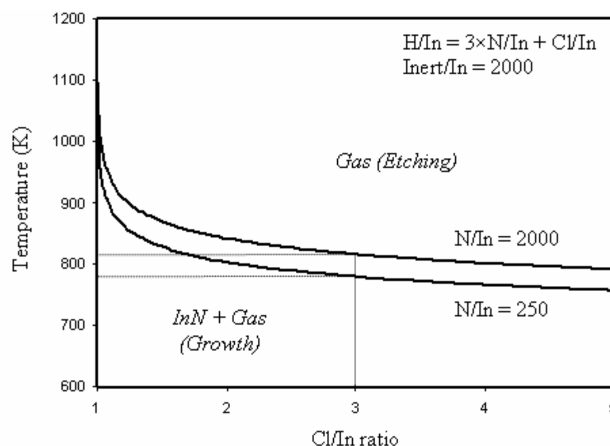


**Figure 4** CVD phase diagram for InN growth.

**4 Conclusions** As a probable mechanism for the catalyst- and template-independent InN nanorod growth in H-MOVPE, a random nanoparticle nucleation from stable gas phase oligomers and the subsequent directional growth along the c-axis were proposed. The computationally resolved growth conditions based on the proposed mechanism had a good agreement with reported experimental results.

Using computational thermochemistry, gas phase reactions ranging from the decomposition of In metalorganic precursors to ammonia adduct formation were investigated to locate a kinetic constraint. A certain high temperature (> 800 K) is necessary to kinetically access the formation of $InCl_3$ as a key species in the proposed mechanism. Despite the high degree of InN etching in the chlorinated environment at high temperatures, the growth zone of InN nanorods by HVPE lied in the vicinity of growth-etch phase boundary where the kinetic constraint was lifted. The important role of $InCl_3$ in the proposed mechanism required a preferable Cl/In ratio of ~ 3. A similar approach will be carried out for GaN and AlN nanorods grown lack of catalyst and template to corroborate the proposed mechanism in group III-nitride nanorod growth.

**Acknowledgements** This work was supported by Samsung Electromechanic Co. Ltd.

## References

[1] J. Sánchez-Páramo, J. Calleja, M. Sánchez-Garcia, and E. Calleja, Physica E **13**, 1070 (2002).

[2] E. Calleja, M. Sánchez-Garcia, F. Sánchez, F. Calle, F. Naranjo, E. Muňoz, U. Jahn, and K. Ploog, Phys. Rev. B **62**, 16826 (2000).

[3] J. Ristic, E. Calleja, M. Sánchez-Garcia, F. Ulloa, J. Sánchez-Páramo, J. Calleja, U. Jahn, A. Trampert, and K. Ploog, Phys. Rev. B **68**, 125305 (2003).

[4] J. Wang, M. S. Gudiksen, X. Duan, Y. Cui, and C. M. Lieber, Science **293**, 1455 (2001).

[5] J. C. Johnson, H.-J. Choi, K. P. Knutsen, R. D. Schaller, P. Yang, and R. J. Saykally, Nature **1**, 106 (2002).


© 2008 WILEY-VCH Verlag GmbH & Co. KGaA, Weinheim

[6] L. J. Lauhon, M. S. Gudiksen, D. Wang, and C. M. Lieber, Nature **420**, 57 (2002).
[7] S. Dhara, A. Datta, C. T. Wu, Z. H. Lan, K. H. Chen, Y. L. Wang, L. C. Chen, C. W. Hsu, H. M. Lin, and C. C. Chen, Appl. Phys. Lett. **82**, 451 (2003).
[8] J. W. Chiou, J. C. Han, H. M. Tsai, W. F. Pong, M. H. Tsai, I. H. Hong, R. Klauser, J. F. Lee, C. W. Hsu, C. C. Chen, C. H. Shen, L. C. Chen, and K. H. Chen, Appl. Phys. Lett. **82**, 3949 (2003).
[9] O. Kryliouk, H. J. Park, H. T. Wang, B. S. Kang, T. J. Anderson, F. Ren, and S. J. Pearton, J. Vac. Sci. Technol. B **23**(5), 1891 (2005).
[10] X. F. Duan and C. M. Lieber, J. Am. Chem. Soc. **122**, 128 (2000).
[11] C. H. Liang, C. L. Chen, J. S. Hwang, K. H. Chen, Y. T. Hung, and Y. F. Chen, Appl. Phys. Lett. **19**, 423 (2004).
[12] H. Y. Peng, X. T. Zhou, N. Wang, Y. F. Zheng, L. S. Liao, W. S. Shi, C. S. Lee, and S. T. Lee, Chem. Phys. Lett. **327**, 263 (2000).
[13] M. K. Sunkara, S. Sharma, R. Miranda, G. Lian, and E. C. Dickey, Appl. Phys. Lett. **79**, 1546 (2001).
[14] C. N. R. Rao, F. L. Deepak, G. Gundiah, and A. Govindaraj, Prog. Solid State Chem. **31**, 5 (2003).
[15] H. M. Kim, D. S. Kim, Y. S. Park, D. Y. Kim, T. W. Kang, and K. S. Chung, Adv. Mater. **14**(13-14), 991 (2002).
[16] O. Kryliouk, H. J. Park, Y. S. Won, T. J. Anderson, A. Davydov, I. Levin, J. H. Kim, and J. A. Freitas, Nanotechnol. **18**(13), 135606 (2007).
[17] J. Yang, T.-W.. Liu, C.-W. Hsu, L.-C. Chen, K.-H. Chen, and C.-C. Chen, Nanotechnol. **17**, S321 (2006).
[18] A. Y. Timoshkin and H. F. Schaefer III, The Chemical Records **2**, 319 (2002).
[19] A. Y. Timoshkin, H. F. Bettinger, and H. F. Schaefer III, J. Am. Chem. Soc. **119**, 5668 (1997).
[20] Y. Okamoto, J. Cryst. Growth **191**, 405 (1998).
[21] A. Y. Timoshkin, H. F. Bettinger, and H. F. Schaefer III, Inorg. Chem. **41**, 738 (2002).
[22] A. Kovács, Inorg. Chem. **41**, 3067 (2002).
[23] Gaussian 03, Revision C.02, M. J. Frisch et al. Gaussian Inc., Wallingford CT, 2004.
[24] A. D. Becke, J. Chem. Phys. **98**, 1372 (1993).
[25] W. Y. Lee, J. R. Strife, and R. D. Veltri, J. Am. Ceram. Soc. **75**, 2803 (1992).
[26] B. Sundman, B. Janson, and J. O. Anderson, CALPHAD: Compt. Coupling Phase Diagrams Thermochem. **9**, 153 (1985).
[27] I. Barin, Thermochemical Data of Pure Substances (VCH, Weinheim, Germany, 1989).
[28] O. Kubaschewski, C. B. Alcock and P. J. Spencer, Materials Thermochemistry (Pergamon Press, Oxford, U.K., 1996).
[29] NIST-JANAF, Thermochemical Tables, 4th ed., edited by J. M. W. Chase (American Chemical Society and the American Institute of Physics, New York, 1999).
[30] A. Y. Timoshkin and H. F. Schaefer III, J. Am. Chem. Soc. **126**, 12141 (2004).
[31] A. Y. Timoshkin, H. F. Bettinger, and H. F. Schaefer III, J. Phys. Chem. A **105**, 3240 (2001).
[32] X. Liu, X. Wu, H. Cao, and R. P. H. Chang, J. Appl. Phys. **95**(6), 3141 (2004).
[33] B. H. Cardelino, C. E. Moore, C. A. Cardelino, D. O. Frazier, and K. J. Bachmann, J. Phys. Chem. A **105**, 849 (2001).
[34] C. J. Cramer, Essentials of Computational Chemistry (John Wiley & Sons, Chichester, U.K., 2002).
[35] J. Leitner, P. Marsık, D. Sedmidubsky, and K. J. Ruzicka, Phys. Chem. Solids **65**, 1127 (2004).
[36] S. W. Kang, H. J. Park, Y. S. Won, O. Kryliouk, T. J. Anderson, D. Khokhlov, and T. Burbaev, Appl. Phys. Lett. **90**, 112616 (2007).

© 2008 WILEY-VCH Verlag GmbH & Co. KGaA, Weinheim